Journal of the European Ceramic Society **19** (1999) 1847–1857

PII: S0955-2219(99)00004-7
0955-2219/99/$ - see front matter

Phase Development in La_2O_3 Doped Al_2O_3:TiO_2 Ceramic Membranes

U. Stefan Björkert,[a] Ramani Mayappan,[b] Diane Holland[a]* and Mike H. Lewis[a]

[a]Centre for Advanced Materials, Department of Physics, University of Warwick, Coventry CV4 7AL, UK
[b]MARA Institute of Technology, Perlis Branch, 02600-Perlis, Malaysia

(Received 14 November 1998; accepted 12 December 1998)

Abstract

The phase development of sol derived diphasic Al_2O_3:TiO_2 membranes doped with La_2O_3 is described together with their pore structure and microstructure. These nanostructrual membranes have been characterised using ^{27}Al MAS–NMR, TEM, BET, XRD and thermal analysis in an attempt to derive a comprehensive description. The membrane materials have been subjected to heat treatments ranging from 275°C to 1200°C in air. Doping the diphasic membrane has been shown to increase the transformation temperature of the low temperature phases (γ-alumina and anatase) by as much as 200°C. There is indication that La_2O_3 doping also retards the reorganisation of Al in the γ-alumina phase preventing it from forming other intermediate aluminas. © *1999 Published by Elsevier Science Limited. All rights reserved*

Keywords: sol–gel processes, porosity, Al_2O_3, TiO_2, xmembranes

1 Introduction

It has been proposed that 'greenhouse' gases can be removed from power station emissions, using permselective membranes. In order to utilise the thermal energy in the exhaust gas for the subsequent CO_2 fixation, the separation process has to be at an elevated temperature (300–600°C). Microporous metal oxide membranes have the capability to operate at these temperatures. However, their efficiency as permselective membranes is dependent on their having, and retaining, a certain pore size and a narrow pore size distribution. Hence, it is necessary to thermally stabilise the membrane material to prevent coarsening of the pore structure at the operating temperature.

Many research groups have shown, both theoretically and experimentally, the benefit of chemisorption of the permeate on the membrane material in order to achieve separation.[1–3] The process that has been observed is that the permeate specie is adsorbed onto the pore wall of the membrane material and then transported by surface diffusion driven by the pressure differential. However, in order to have any beneficial effects, the chemical interaction must still be present at the operating temperature of the membrane. So far research has only been able to demonstrate this effect at room temperature.

This study has been concerned with thermally stabilising an alumina membrane microstructure with a titania second phase and stabilising the phase composition by doping with lanthanum oxide which should also enhance the chemical interaction between the membrane material and CO_2.

2 Experimental Procedures

The lanthanum-oxide doped alumina/titania material was produced using aluminium sec-butoxide, titanium(IV) iso-propoxide and lanthanum nitrate as precursors. All the precursors were standard commercial AR grade chemicals from Aldrich Chemical Co., England. Two sols were made and hydrolysed separately, a titanium-alkoxide and an aluminium-alkoxide sol. The aluminium sec-butoxide sol followed Yoldas[4] preparation route in two steps, first hydrolysis followed by peptization, both at 90°C. The molar ratio of water to alkoxide and molar ratio of HCl to alkoxide were 100 and 0·25 respectively. Lanthanum nitrate was added, to the hydrolysis step of the boehmite sol, so that the ratio of added lanthanum ions to the sum of Al- and Ti-ions [i.e. $r = n_{La}/(n_{Al} + n_{Ti})$] would be 0,

*To whom correspondence should be addressed. E-mail: d.holland@warwick.ac.uk

0·05, 0·1 and 0·15. However, for the titanium(IV) iso-propoxide sol, only a single hydrolysis step was used (at 80°C). In this case the molar ratio of water to alkoxide and HNO_3 to alkoxide were 300 and 0·5 respectively. The amount of metal ion in the Ti-alkoxide sol was adjusted, with iso-propanol, to a concentration of $1{\cdot}6\times10^{-1}$ mol l^{-1}. These two sols were mixed to make up compositions of 95, 90 and 85 mol% Al_2O_3 (the rest TiO_2) in the final pyrolysed material and the total metal ion concentration was adjusted to 4×10^{-1} mol l^{-1} in all sols, by adding water.

A xerogel was produced by drying the sol in an oven at 50°C in an atmosphere of air until dry. This was normally achieved in a week. These xerogels were then further heat treated, in air, to 275, 325, 600, 800, 900, 1000, 1100 and 1200°C with a slow heating rate (1°C min^{-1}) from room temperature and held at temperature for 3 h.

X-ray diffraction (XRD) and transmission electron microscopy (TEM) together with magic angle spinning nuclear magnetic resonance (MAS–NMR) of powders have been used to examine the phase development and the microstructure in these materials. Thermal analysis, including differential thermal analysis (DTA) and thermogravimetric analysis (TGA), was performed on powdered xerogels to obtain information on their crystallisation and transformation temperatures. The TGA was done on a Stanton Redcroft TG 750 with a sample weight of around 25 mg and a heating rate of 10°C min^{-1} up to 1000°C. The DTA data was collected on a Netzsch DSC 404 heating at 10°C min^{-1} from room temperature to 1500°C. The sample weight was in these cases around 80 mg in a platinum/rhodium crucible. Quartz was used as the reference material. All the thermal analysis was performed in air.

TEM was done on finely ground powder which was ground in iso-amyl-acetate. A drop of the final powder/iso-amyl-acetate suspension was deposited onto a carbon film coated, copper grid and left to dry in air. The TEM images were collected on a JEOL JEM2000FX working at 200 kV and the pore structure was imaged using a defocusing technique as described by Kerch *et al.*[5]

A Philips PW1130 diffractometer fitted with a step scanner, was used to record the XRD data. Copper K_α radiation was used together with a step increment of 0·01 °2θ. For crystal size calculation, the peaks in the XRD data were first fitted with a theoretical curve for an estimation of peak centre and peak full width at half maximum height (FWHM). The theoretical curve treated Cu$K_{\alpha1}$ and Cu$K_{\alpha2}$ as two superimposed pseudo-Voigt functions with a separation determined by the 2θ-value. Furthermore, a constant ratio between the two peak intensities ($I_{\mathrm{Cu}K_{\alpha2}}/I_{\mathrm{Cu}K_{\alpha1}} = 0{\cdot}51$) was assumed. The peak centre and the FWHM were subsequently used in the Scherrer relationship:

$$D_{\mathrm{hkl}} = K\lambda/(\beta_{\mathrm{hkl}}\cos\theta) \tag{1}$$

where λ is the wavelength of the X-ray radiation and K is a constant which depends on many factors, including the shape of the crystals. A value of 0·89 for K was assumed. β_{hkl} is the FWHM of the peak after correction for the instrumental line broadening. There are several ways to take the instrumental line broadening into account. One suggested by Warren and Taylor[6] and the one used in this study is:

$$\beta_{\mathrm{hkl}} = \sqrt{B^2 - b^2} \tag{2}$$

where B is the FWHM of the peak and b is the instrumental line broadening. The instrumental line broadening was obtained from FWHM of peaks in the same angular region for a polycrystalline $\alpha-Al_2O_3$ sample with crystal size $> 1\,\mu$m.

The ^{27}Al MAS-NMR spectra were collected at 93·8 MHz on a Bruker MSL 360 using a spinning speed of 10 kHz, a pulse length of 1 μs and a delay of 1 s. For the interpretation of the spectra, the area underneath the produced peaks has been estimated by fitting each peak with a pseudo-Voigt function with different FWHM on either side of the peak centre. (In the case of the five co-ordinated Al it was found that there was not enough information in the spectrum to have the FWHM on either side of the centre varying and was therefore put equal on both sides.) This is, however, a very crude measurement of the area since the quadrupolar line shape will depend on the field gradients and asymmetry parameters of the different Al sites. These parameters are extremely difficult to quantify, so, although the chosen peak shape has inadequacies and, therefore large associated errors, it will give qualitative information on the number of Al ions with different co-ordination. However, it will give a better estimate than a simple integration of the area underneath each peak, as it takes into account the overlap that exists between the peaks.

Pore size and pore size distribution were characterised using gas adsorption/desorption on a Micromeritics ASAP 2000, followed by Brunauer, Emmett and Teller (BET) analysis. These results were compared with the visual results obtained from TEM.

3 Results and Discussion

3.1 XRD

XRD data from a xerogels show the presence of pseudo-boehmite (γ-$Al_2O_3{\cdot}1{\cdot}3H_2O$). Anatase ($TiO_2$)

is also present in the spectrum of the undoped samples. However, the line width is very broad for the pseudo-boehmite. With increasing La_2O_3 content the boehmite peaks broaden even further, indicating either smaller crystallites or a more disordered form of boehmite which contains lanthanum ions. At a processing temperature of 600°C the XRD trace of undoped material [Fig. 1(a)] showed, in addition to anatase (5), peaks at *d*-values of 1·40, 1·98 and 2·38 Å (1). There are several transition aluminas and all of them have strong reflections at ~1·40 and ~1·98 Å.[7] However, the positions and relative intensities match those of γ-alumina.[8] With further heat treatment, 900°C and higher, a transformation of the γ-alumina to the high temperature α-alumina phase (2) is observed and similarly a transformation of the anatase phase to rutile (6). However, there is little evidence that the γ to α transition goes via the other transitional aluminas (δ and θ) as reported by Wilson.[9–11]

For the higher levels of La_2O_3 dopant ($r = 0{\cdot}10$ and 0·15), Fig. 1(b), there is an initial transformation to γ-alumina from the pseudo-boehmite but the diffraction peaks remain very broad. At a processing temperature of 1000°C strong peaks appear corresponding to *d*-values of 1·34, 1·55, 1·90, 2·19, 2·68 and 3·79 Å (4). The relative intensity and the position of these peaks agree very well with those from $LaAlO_3$.[12] Reflections of this phase appear at lower processing temperature with increasing La_2O_3 content in the sample. However, in the 85 mol% Al_2O_3 material there is a slight shift in the peak position towards lower 2θ-values, corresponding to an increase in *d*-spacing. Lanthanum aluminate possesses a rhombohedral distorted perovskite crystal structure [space group R3mR (160)] which is closely related to the cubic system ($\alpha = 90{\cdot}1°$).[13] Lanthanum titanate, $LaTiO_3$, has, also, a near perovskite structure belonging to the Pm-3m (221) space group[14] and, hence, has almost the same atomic positions as in lanthanum aluminate

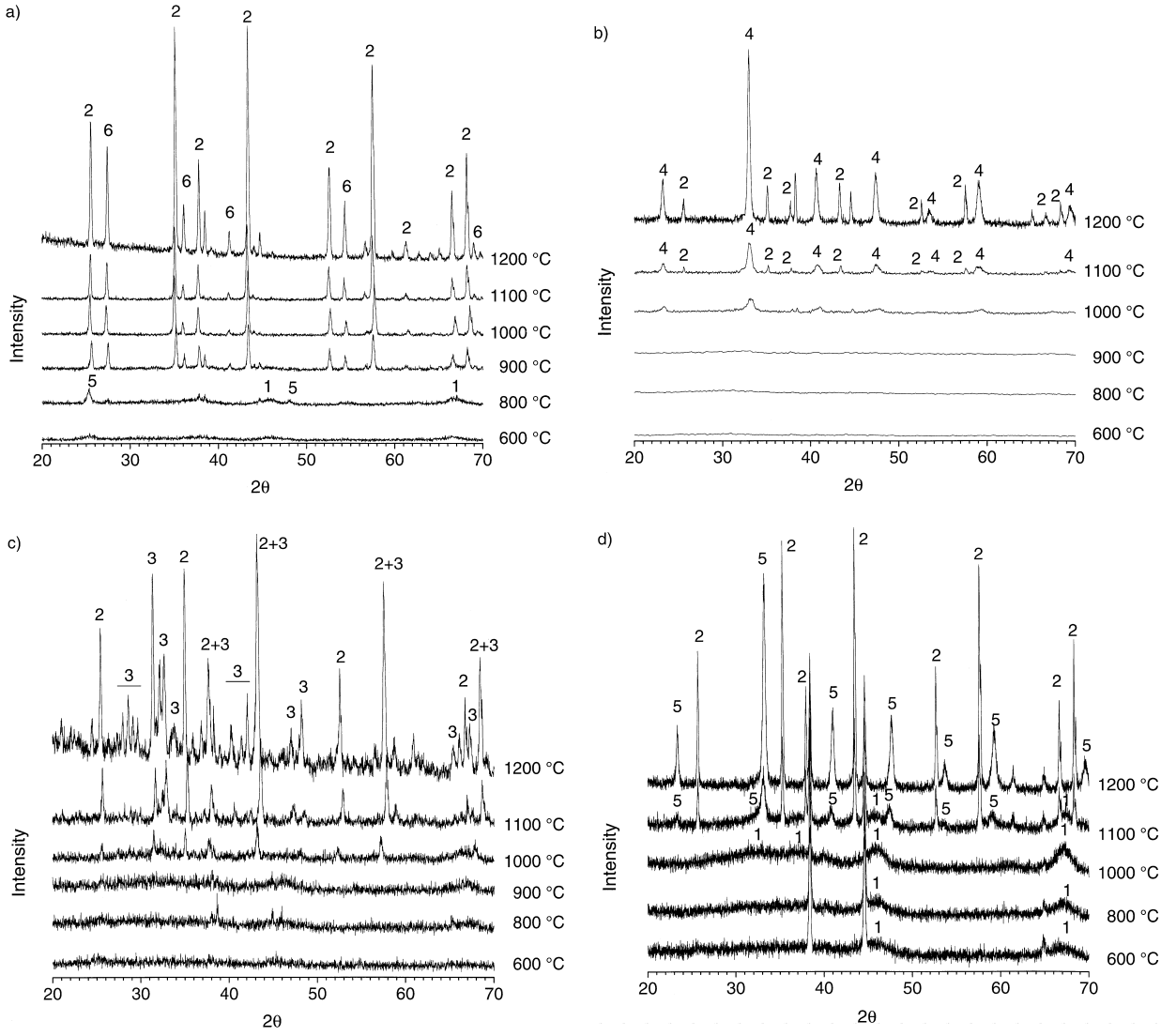

Fig. 1. XRD traces of 85 mol% Al_2O_3: (a) $r = 0$, (b) $r = 0{\cdot}15$, (c) $r = 0{\cdot}05$ and (d) 95 mol% Al_2O_3 $r = 0{\cdot}05$ at various processing temperatures. Key: 1. γ-alumina; 2. α-alumina; 3. $La_3Ti_5Al_{15}O_{37}$; 4. $LaAlO_3/LaTiO_3$ solid solution; 5. anatase and 6. rutile.

but with larger lattice parameter (3·92 Å compared with 3·79 Å). This would mean that there is a reasonable chance that these two phases could enter into a solid solution. Assuming that we have a solid solution of these two phases, one can calculate the relative proportions of the two phases using the lattice parameter of the solid solution. Refining the cell parameters for 85 mol% Al_2O_3 and $r = 0{\cdot}15$ powders pyrolysed at 1100 and 1200°C, using a hexagonal setting, the lattice constants were found to be 3·83 Å with an angle of 90·1° between the axes in the rhombohedral cell. This, in turn, means a 30% substitution of Ti-ions for Al-ions in $LaAlO_3$, assuming that Vegard's law is applicable. At 1100 and 1200°C α-alumina is also present in the XRD traces. The onset of formation of α-alumina is dependent on the level of La_2O_3 in the sample, moving to higher temperatures as the concentration increases.

A slightly different picture is seen in the material with 85 mol% Al_2O_3 when the La_2O_3 dopant is low, $r = 0{\cdot}05$, see Fig. 1(c). After the transformation of pseudo-boehmite to γ-alumina at the lower processing temperatures (800 and 900°C) we see a number of peaks appearing when the material is pyrolysed at 1000°C and becoming more prominent at higher processing temperature. However, we do not see any significant trace of anatase at the lower processing temperature unlike the material with no lanthanum oxide. The resulting spectrum has been identified as containing peaks from two phases, α-alumina and $La_3Ti_5Al_{15}O_{37}$ (LTA). The LTA phase (3) is the same phase which Morgan[15] was trying to prepare using a sol-gel route and was found to form at about 1000°C. However, Morgan formulated the phase as $LaTi_2Al_9O_{19}$ but later revised it to $La_3Ti_5Al_{15}O_{37}$.[16] This significant difference in phase development for samples with low La_2O_3 doping ($R = 0{\cdot}05$) was not observed in the higher alumina compositions, see Fig. 1(d), which, followed the same trend as seen in the higher r value systems, i.e. γ-alumina undergoing transition to α-alumina with the formation of lanthanum aluminate at high processing temperature. However, in the $r = 0{\cdot}05$ material, the formation of lanthanum aluminate starts at a higher processing temperature of 1100°C while the transformation from γ- to α-alumina has already started at 1100°C.

In Fig. 2, the results from crystal size calculations for some phases are plotted versus process temperature. Evident from the graph is that the transformations from γ-alumina and anatase, to their high temperature phases are associated with crystal growth and a coarsening of the microstructure. This is not unexpected as these transformations involve a nucleation process and a complete reconstruction of the oxygen lattice. The line broadening of the γ-alumina reflections in La_2O_3 doped samples is reflected in the decreasing crystal size for the phase as the doping level is increased, see Fig. 3. Whether this is a true decrease in the crystal size or whether it is a loss of long-range order due to distortion of the γ-alumina crystal structure as a result of incorporation of large La-ions in the perovskite structure is not confirmed. However, TEM showed no significant decrease in crystallite size, hence, it seems more likely that the broadening of the XRD diffractions is caused by solid-solution of La_2O_3 and γ-alumina.

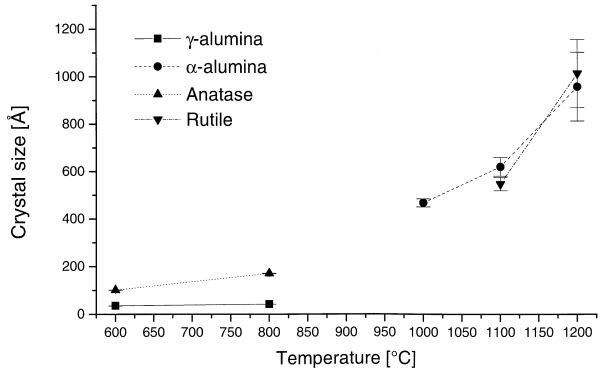

Fig. 2. Graph showing the crystallite size calculated using XRD data for γ-alumina, α-alumina, anatase and rutile versus process temperature for the undoped 95 mol% Al_2O_3 sample.

3.2 DTA and TGA

From the DTA (Fig. 4) four endothermic peaks can be seen (peaks labelled 1-4) and three exothermic peaks (5–7). TGA (Fig. 5) shows that all of the endothermic features are associated with weight loss. The first peak has been identified as corresponding to evaporation of physically bound water. Peak 2 is more complex as it decreases dramatically between samples with $r = 0$ and 0·05 and does not seem to change with further increase of r. Peak 3 is not observed for $r = 0$ but increases in size and shifts towards higher temperature with increasing La_2O_3 doping. Peak 4 decreases with

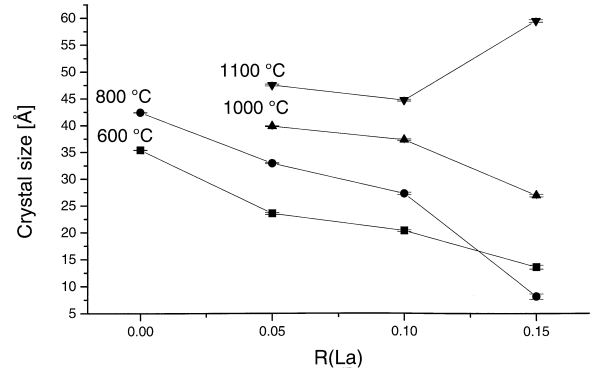

Fig. 3. Graph showing the crystallite size calculated using XRD data for the γ-alumina phase, in samples with different degrees of doping, at four processing temperatures.

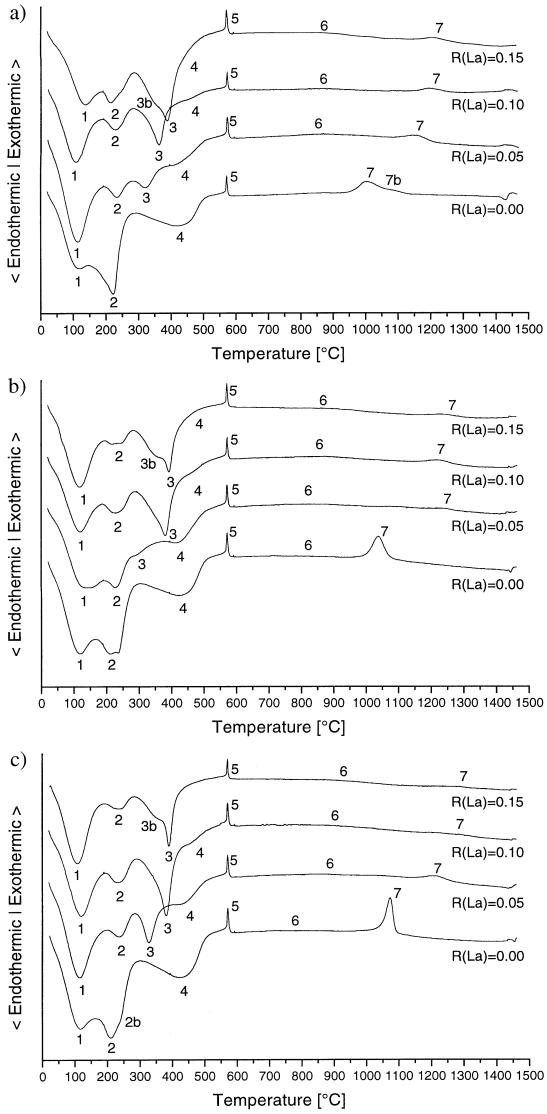

Fig. 4. DTA traces from (a) 85 mol%, (b) 90 mol% and (c) 95 mol% Al_2O_3, for the four different doping levels, versus temperature.

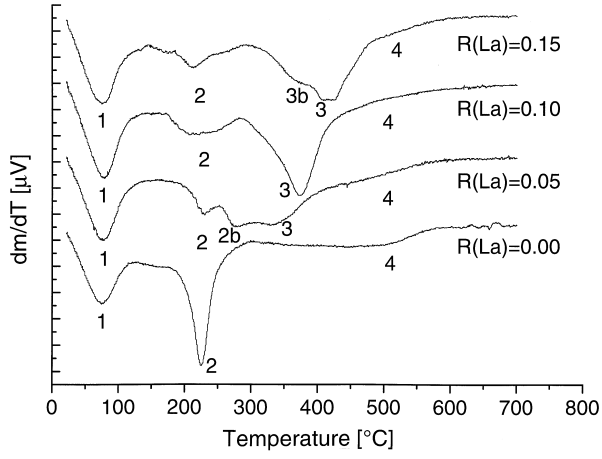

Fig. 5. TGA traces of 95 mol% Al_2O_3 for the four different doping levels versus temperature.

added La. From NMR and XRD data two phases, pseudo-boehmite (γ-$Al_2O_3 \cdot 1{\cdot}3H_2O$) and γ-alumina (γ-Al_2O_3), are observed in this temperature region. This suggests that peaks 3 and 4 are part of the pseudo-boehmite to γ-alumina transition. The transformation temperature of boehmite to γ-alumina is reported to be between 400 and 450°C and involves removal of hydroxyl groups by cleavage of O–H–O bonds, a time and energy consuming process.[10] Hence, a possible interpretation of the endothermic region in the DTA is that peak 4 is related to the transformation of boehmite to γ-alumina as it is broader and has a larger area then peak 3. That leaves peak 3 to be related to the loss of the extra water of crystallisation from pseudo-boehmite giving boehmite. If this interpretation is correct, then La ions appear to retard the pseudo-boehmite to boehmite transition, giving rise to a shift in this peak towards higher temperature as La_2O_3 doping levels increase and the apparent peak 2 for the $r = 0$ samples is really a combination of the loss of water of crystallisation in pseudo-boehmite (peak 3 in other samples) and the second endothermic peak due to the decomposition of nitrates (peak 2 for all the other r's). The gradual decrease in peak 4 between $r = 0$ and 0·15 can be explained by chemical interaction between La and boehmite, leading to consumption of this phase before transformation to γ-alumina can occur.

The first apparent exothermic peak, labelled 5, is the α-SiO_2 to β-SiO_2 endothermic phase transformation in the reference material. The part of the DTA trace that has been labelled 6 is a very broad peak which has its onset at about 650°C and tails out just before the onset of peak 7. This peak increases with increasing La_2O_3 content suggesting that it could also be a result of the formation of various La containing phases as seen in the XRD data (i.e. $LaAlO_3$ and $LaTiO_3$ or $LaTi_2A_{19}AO_{19}$ in the case for 85 mol% Al_2O_3 $r = 0{\cdot}05$).

Peak 7 corresponds to the transformation of the low temperature aluminas to α-alumina. The area under this peak decreases with increasing La_2O_3 doping in the material. This is consistent with the observation in peak 6, i.e. that the γ-alumina is consumed by the formation of $LaAlO_3$. In Fig. 6 the extrapolated onset temperature of the γ- to α-alumina transformation is shown as a function of La_2O_3 doping. It clearly shows that the transformation temperature is increased by as much as 200°C with La_2O_3 doping. This is important as the α-alumina transformation is a nucleation and growth process and, hence, associated with coarsening of the microstructure and the disappearance of nano-pores as observed in the TEM. Furthermore, a noticeable trend is that the transformation temperature decreases with the amount of TiO_2 in the material indicating that TiO_2 either catalyses the γ- to α-alumina transformation or provides convenient nucleation sites. Noteworthy in Fig. 6 is

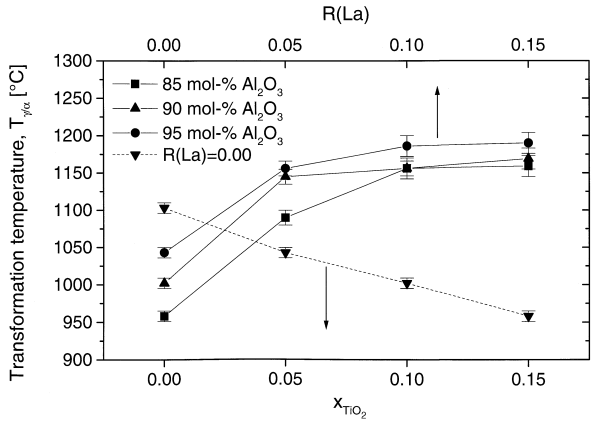

Fig. 6. Graph showing the extrapolated onset for the γ- to α-alumina transformation temperature with respect to mol% TiO_2 in the sample (broken line and lower x-axis) and doping level (solid lines and upper x-axis).

that the transformation temperature of xerogels containing pure pseudo-boehmite (i.e. 100 mol% Al_2O_3 and $r = 0{\cdot}00$) is 1103 ± 7°C.

3.3 BET

In Fig. 7(a) the BET surface area and the average pore diameter have been plotted against the doping level in samples processed at 600 and 800°C. The results show that the surface area of the samples decreases gradually with increasing amount of doping in a nearly linear fashion. Equally, the surface area decreases when the processing temperature is increased. Both the 600°C and the 800°C curves have similar slopes indicating that La_2O_3 has little or no influence on the reduction of surface area as a function of process temperature.

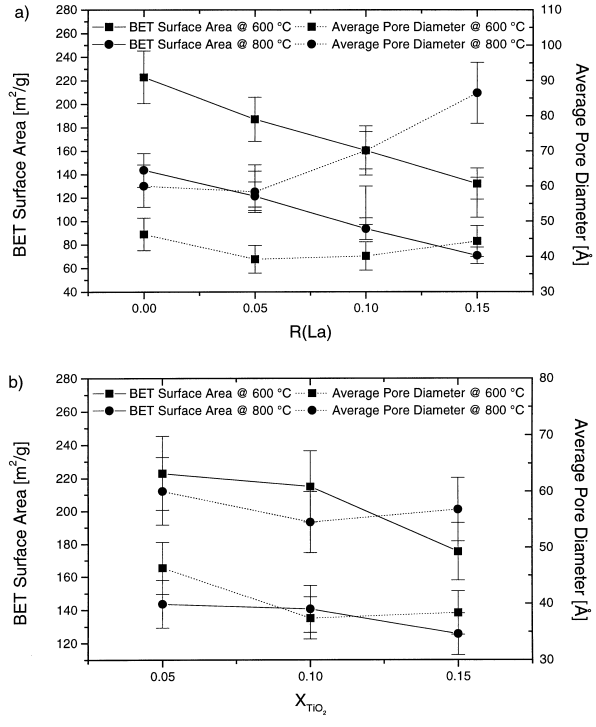

Fig. 7. Graph showing the results from N_2-gas physisorption: BET surface area (solid lines and left y-axis) together with average pore diameter (broken line and right y-axis) versus (a) doping level and (b) versus mol% TiO_2.

At 600°C the pore size is fairly constant, around 42 Å, with respect to the doping level in the sample. However, at 800°C the increase in pore size seems to be accelerated by increasing concentration of La_2O_3. The undoped material has a pore size of 60 Å whereas for $r = 0{\cdot}15$ the pore size has increased to 86 Å. At both temperatures there is a reduction of 29% in pore volume between $r = 0$ and $r = 0{\cdot}15$. From the BET measuments it is also clear that there is only a small decrease in both pore size and surface area with increasing TiO_2 ratio, see Fig. 7(b). The surface area is reduced significantly and the pore size increased when the membrane material is exposed to a higher process temperature.

3.4 TEM

Phase identification using TEM is consistent with the results from the XRD data. At 600°C the microstructure in the membrane material is highly microporous. The morphology and pore structure of the material can be seen in the micrographs in Fig. 8a. From energy dispersive X-ray (EDX) analysis the material was found to contain both alumina and titania. From XRD it was noted that at 600°C there are two phases present, namely anatase and γ-alumina, and that they contain small crystallites (~100 and ~35 Å, respectively). Hence, this implies that the porous microstructure seen in Fig. 8 consists of the desired two phase material. The pore size is fairly uniform across the spectrum of doping level at this temperature and the size was measured to be roughly 50–55 Å. From a dark field image, Fig. 8(b), of the undoped 95 mol% Al_2O_3 the crystallite size can be estimated to be 61 Å. This is roughly the average crystallite size for the two phases calculated from the XRD data. At high doping levels ($r = 0{\cdot}10$ and $0{\cdot}15$) small amounts of $LaAlO_3$ are also seen. However, this only constituted a few percent by volume of the material, increasing in the samples processed at 800°C but still within 5–10%. It was also noted that the pore size had increased slightly to about 55–60 Å. Furthermore, the formation of $LaAlO_3$ was accompanied by a coarsening of the microstructure and, hence, loss of pore volume and an increase in pore size.

At a processing temperature of 1000°C it was found that α-alumina had started forming in the material with no doping or with $r = 0{\cdot}05$. As can be seen in Fig. 8(c), this results in severe coarsening of the microstructure and a loss of pore volume as a result. The crystallite size measured in these cases was around 935 Å. This is consistent with XRD observations, see Fig. 3.

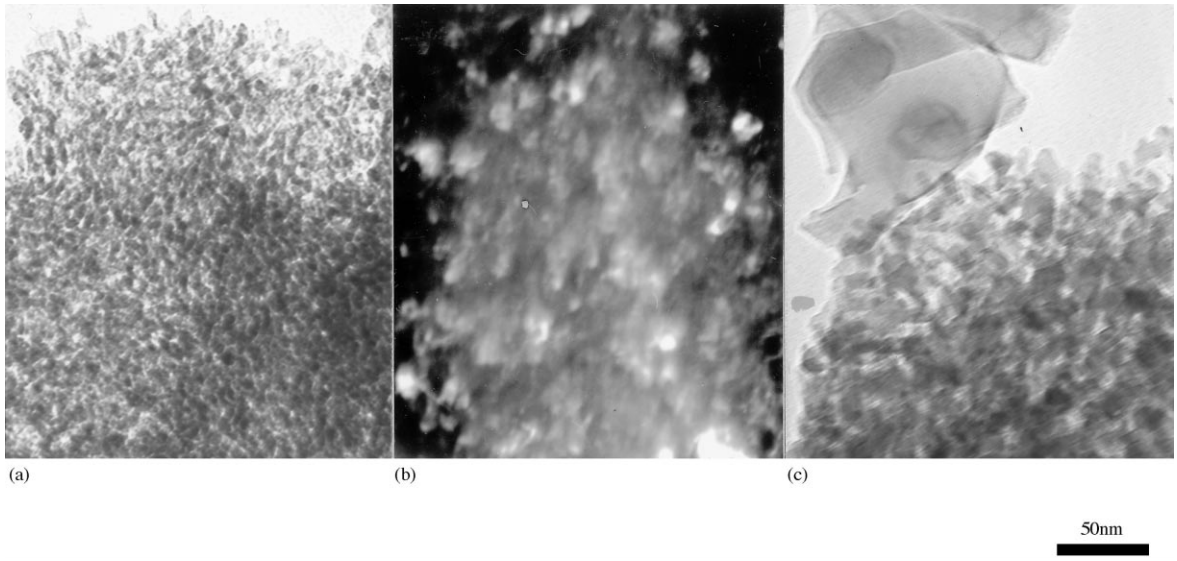

Fig. 8. TEM micrograph showing (a) an under-focused bright-field image, (b) a dark-field image of the microstructure of membrane material for 95 mol% Al_2O_3 $r = 0$ processed at 600°C and (c) an under-focused image of microstructure in the 95 mol% Al_2O_3 $r = 0{\cdot}05$ at 1000°C (α-alumina at the edge of a porous region).

3.5 ^{27}Al MAS NMR

The NMR spectra are summarised in Fig. 9. At low processing temperatures, below the full transformation of pseudo-boehmite to γ-alumina at 450°C, NMR shows a single, broad, asymmetric peak with its centre of gravity around 4 ppm. This peak corresponds to six co-ordinated aluminium and the line shape is the result of interaction between the quadrupole moment of the nucleus and the field gradient resulting from the asymmetric charge distribution around the Al site in boehmite. Boehmite has a layered structure where aluminium has six nearest neighbours consisting of five oxygen and one hydroxyl group,[10] which creates the asymmetry. Furthermore, the phase produced in the xerogel is pseudo-boehmite rather then pure boehmite which means that it contains additional water of crystallisation.[17]

NMR spectra of samples heat treated above the transition temperature for pseudo-boehmite show a second asymmetric peak at around 64 ppm corresponding to four co-ordinated aluminium in tetrahedral sites, which is expected for γ-alumina. An additional peak is present at 27 ppm in samples processed at 600 and 800°C. Furthermore, this peak is more pronounced in La_2O_3 doped samples. Mizushima and co-workers[18] found a similar peak in their NMR spectra of alumina aerogels and assigned it to five co-ordinated aluminium. The presence of five co-ordinated aluminium on the surface of γ-alumina has also been suggested by Chen *et al.*[19] from ^{27}Al MAS–NMR. Furthermore, five co-ordinated Al has been shown theoretically by Alvarez *et al.*,[20] using molecular dynamic simulations, to exist in the bulk and on the surface of γ-alumina. Hence, this peak has been assigned to five co-ordinated aluminium.

At higher processing temperatures, the peak corresponding to four co-ordinated aluminium also disappears and there is a shift in the peak for the six co-ordinated aluminium to a centre of gravity of around 12 ppm. Furthermore, the peak becomes symmetrical, as expected for Al in α-alumina. The transition temperature between these two types of spectrum depends on the amount of La_2O_3 in the sample. With increased La_2O_3 in the sample the transition temperature increases, reflecting the results obtained from the DTA data for the formation of α-alumina.

The results from the fitting of the NMR data show some general trends. four co-ordinated Al is mostly present around processing temperatures of 600–1000°C and is retained to a higher temperature with increasing La_2O_3 doping, before re-organisation of the structure to form α-alumina.

In Table 1 the proportions of four, five and six co-ordinate aluminium, averaged over the different doping levels, are presented for various temperatures. At these temperatures the proportions are almost constant across the four doping levels within the uncertainty of the measurements. There is no indication of γ-alumina undergoing any transformation in the 600 to 800°C temperature region, apart from a slight change in the proportion of four co-ordinated Al in the 85 mol% between 600 and 800°C (which results from exceptional values for the $r = 0{\cdot}05$ material). This suggests that there is no phase transition taking place in the material and the alumina contains four co-ordinated aluminium ranging form 21 to 31%, five co-ordinated ranging from 6·5 to 7% and six co-ordinated ranging from 62 to 72%.

Both in the low and high temperature region (50 and 1200°C) the majority of the aluminium ions

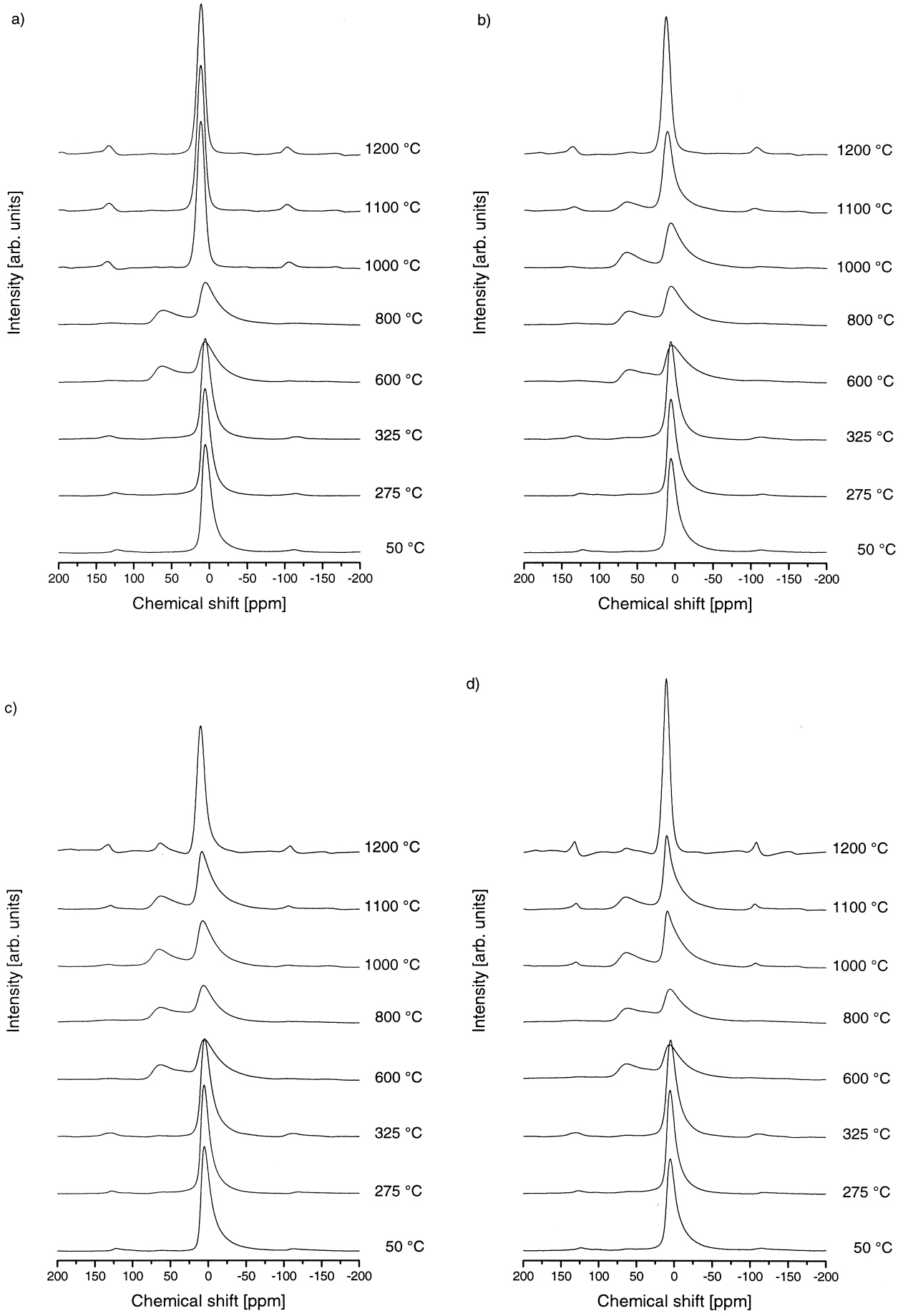

Fig. 9. Graphs showing the results from ^{27}Al MAS–NMR of 95 mol% Al_2O_3: (a) $r = 0$, (b) $r = 0{\cdot}05$, (c) $r = 0{\cdot}1$ and (d) $r = 0{\cdot}15$ for the different processing temperatures.

Table 1. Average proportion of four, five and six co-ordinated aluminium over the four different La_2O_3 doping levels

Composition	*Temperature °C*	*Percentage of Al with a given co-ordination number*		
		Four	*Five*	*Six*
85 mol% Al_2O_3	50	2·0	0·6	97·4
	600	23·3	7·0	69·7
	800	31·1	7·0	61·9
	1200	0·6	0·6	98·8
95 mol% Al_2O_3	50	1·0	0·0	99·0
	600	21·3	6·5	72·2
	800	21·3	6·7	72·0
	1200	5·8	0·0	94·2

Table 2. Fraction of four, five and six co-ordinated aluminium in crystalline phases

Key	*Phase*		*Al co-ordination number*			
			Four	*Five*	*Six*	*Ref.*
B	Pseudo-boehmite		0	0	1	9
		Tetrahedral vacancies	0·25	0	0·75	9
γ	γ-Alimina	Random vacancies	0·33	0	0·67	9
δ	δ-Alumina		0·375	0	0·625	9
θ	θ-Alumina		0·50	0	0·50	9
α	α-Alumina		0	0	1	26
LTA	$LaTi_2Al_9O_{19}$		0·267	0·067	0·667	16
SS	$LaAlO_3$		0	0	1	13

are six co-ordinated. This is not surprising since XRD shows that at 50°C pseudo-boehmite is the dominant alumina phase and at 1200°C lanthanum aluminate and α-alumina are the two dominating aluminium containing phases. In all of these phases, aluminium is six co-ordinated.

4 Overall Discussion

Wilson[9–11] has suggested that the phase transition from γ- to α-alumina goes via two intermediate alumina phases, δ- and θ-alumina (in that order). It has been suggested that their transformation is topotactic and that the difference between these three phases is a reorganisation of aluminium ions in the tetrahedral and octahedral sites in the near spinel crystal structure. The γ-alumina formed from pseudo-boehmite has a tetragonal distortion with predominantly cation vacancies in the tetrahedral sites. There are two competing processes giving rise to the transformation of δ-alumina. First, the realisation of an ideal random distribution of the vacancies which decreases the tetragonal distortion to nearly cubic and, secondly, a reordering on the octahedral sites which increases the tetragonal distortion again. Hence, the cubic state is never reached and the final unit cell is tripled along the c_γ axis. The transformation δ- to θ-alumina involves only a re-arrangement of the cations. This means that each of these three alumina intermediates has their own characteristic proportion of four and six co-ordinated Al ions, as summarised in Table 2. The phase transformation of γ-alumina to θ-alumina via δ-alumina is not observed in the XRD data. However, all of these three phases have very similar reflections and they are usually found in combination as their transformation ranges overlap each other.[11] It is, therefore, difficult to conclude whether the transformations occur from the XRD data. However, NMR is a highly sensitive technique for characterising the local environment of the probed species. Therefore, it should give an indication whether this re-arrangement of the cations is occurring or not.

The suggested arrangement for the five co-ordinated aluminium is a highly distorted trigonal bipyramid with oxygens in each corner.[21] Two of these polyhedra have the ability to share edges to form a dimer. This is the situation for five co-ordinated aluminium, which has been implied for andalusite. In the light of the suggested aluminium configuration in a five co-ordinated site and the fact that the octahedral site is less stable with respect to the tetrahedral due to the larger bond length (1·91 Å compared with 1·76 Å for tetrahedral configuration[22]), it is reasonable to assume that the majority of the five co-ordinated aluminium is a result of oxygen vacancies in what would have been an octahedral site in the ideal spinel structure. Hence, this implies that about 22% for the aluminium ions are in the tetrahedral sites and 78% originated from octahedral sites. Even if we take into account that some of the tetrahedral sites have formed the five co-ordinated aluminium then this leaves us with roughly a ratio of 25:75 between 4:6 co-ordination as has been suggested for γ-alumina with tetrahedral vacancies,[9] see Table 2. Hence, this, in return, implies that γ-alumina is the predominant phase at this temperature with no significant reorganisation of the aluminium ions.

As demonstrated in the DTA and ^{27}Al MAS–NMR, it is possible to thermally stabilise the low temperature phases of alumina by doping it with La_2O_3. Oudet *et al.* and Lin *et al.*,[23,24] suggest that the stabilising mechanism for La_2O_3 doped alumina is the formation of $LaAlO_3$ on the active nucleation sites on the γ-alumina phase rather than a solid solution of La_2O_3 and Al_2O_3. These active sites would normally be available for the nuclea-

tion of α-alumina and hence the presence of the LaAlO3 phase will inhibit this nucleation. This would mean that even low levels of La_2O_3 doping would have a great effect on the transformation temperature. This is confirmed in the NMR data. Such a mechanism would reach a limit when $LaAlO_3$ has occupied all the available active nucleation sites as seen in the DTA results in this study.

The XRD data indicate lower crystallinity or a decrease in crystallite size for the La_2O_3 doped as compared to the undoped samples. Since a decrease in crystallite size was not observed in TEM, this suggests that a more disordered pseudo-boehmite forms, which contains La ions. The subsequent γ-alumina is also more disordered than the undoped counterpart. This is further supported by the fact that peak 4 of the DTA trace decreases with increased La_2O_3 doping. This complicates the picture presented by Oudet and Lin.[23,24] This fact could also be the explanation as to why this study showed so little rearrangement of the aluminium ions, i.e. the existence of La ions in the γ phase not only distorts it but also locks the Al ions in place. If this is true it would also contribute to the thermal stabilisation of γ-alumina. This effect has been observed by Ozawa *et al.*[25]

5 Conclusions

It has been shown that the thermal stability of the γ-alumina phase can be dramatically improved by doping it with La_2O_3. The major contribution to this improvement is the formation of $LaAlO_3$ on the surface of the alumina phase, hence reducing the number of nucleation sites for the nucleation and growth of α-alumina. However, an additional factor is the formation of a solid solution between La_2O_3 and Al_2O_3 which can be seen in the line broadening in the XRD results and which can, possibly, explain why no reorganisation of the aluminium ions is observed in the doped material in this study.

The postulated microstructural stabilising effect with a secondary titania phase has not been proven because no link between pore size increase and surface area decrease due to higher process temperature was found. However, TiO_2 was shown to have an adverse effect on the γ- to α-alumina transformation temperature by lowering it by as much as 150°C.

Acknowledgements

The authors would like to thank the New Energy and Industrial Technology Development Organization (NEDO), Japan, and Japan Fine Ceramic Center (JFCC) for financial support for this work.

References

1. Furukawa, S.-I. and Nitta, T., Computer simulation of permeation of gas mixtures through carbon membranes using non-equilibrium molecular dynamics, Proceedings of the International Congress on Membranes and Membrane Processes, Yokohama, Japan, Aug. 1996.
2. van de Graaf, J. M., Bakker, W. J. W., Kapteijn, F. and Moulijn, J. A., Unified description of the permeation and separation behavior of silicalite-1 membrane. Proceedings of the International Congress on Membranes and Membrane Processes, Yokohama, Japan, Aug. 1996.
3. Asaeda, M., Tsuru, T., Manabe, T. and Hashimoto, H., Porous silica and silica-zirconia membranes for separation of inorganic gas mixtures including carbondioxide, Proceedings of the International Congress on Membranes and Membrane Processes, Yokohama, Japan, Aug. 1996.
4. Yoldas, B. E., Alumina sol preparation from alkoxides. *Am. Ceram. Soc. Bull.*, 1975, **54**, 289–290.
5. Kerch, H. M., Cosandey, F. and Gerhardt, R. A., Imaging of fine porosity in a colloidal silica: potassium silicate gel by defocus contrast microscopy. *J. Non-Cryst. Solids*, 1993, **152**, 18–31.
6. Taylor, A., An Introduction to X-ray Metallography. Chapman & Hall Ltd, London, 1952.
7. Ervin, G. Jr., Structural interpretation of the diaspore-corundum and boehmite–Al_2O_3 transitions. *Acta Cryst*, 1952, **5**, 103–108 .
8. JCPDS file 10–425.
9. Wilson, S. J., Phase transformation and development in boehmite-derived transition aluminas. *Proc. British Ceram. Soc*, 1979, **28**, 281–294.
10. Wilson, S. J., The dehydration of boehmite, γ-AlOOH, to γ-Al_2O_3. *J. Solid State Chem.*, 1979, **30**, 247–255.
11. Wilson, S. J. and McConnell, J. D. C., A kinetic study of the system γ-AlOOH/Al_2O_3. *J. Solid State Chem.*, 1980, **34**, 315–322.
12. JCPDS file 31–22.
13. Fedulov, S. A., Venevtsev, N. and Dzhmukhadze, D. F., *Kristallografiya*, 1962, 7, 408–411.
14. Kestiginian, M. and Ward, R., *J. Am. Chem. Soc.*, 1954, **76**, 6027.
15. Morgan, P. E. D., Preparing new extremely difficult-to-form crystal structures. *Mat. Res. Bull.*, 1984, **19**, 369–376.
16. Morris, R. E., Owen, J. J., Stalick, J. K. and Cheetham, A. K., Determination of complex structures from powder diffraction data—the crystal-structure of $La_3Ti_5Al_{15}O_{37}$. *J. Solid State Chem.*, 1994, **111**, 52–57.
17. Bagwell, R. B. and Messing, G. L., Critical factors in the production of sol–gel derived porous alumina. *Key Engineering Materials*, 1996, **115**, 45–64.
18. Mizushima, Y., Hori, M. and Sasaki, M., ^{27}Al MAS–NMR spectra of alumina aerogels. *J. Mater. Res.*, 1993, **8**, 2109–2111.
19. Chen, F. R., Davis, J. G. and Fripiat, J. J., Aluminium coordination and lewis acidity in transition aluminas. *J. Catal.*, 1992, **133**, 263–278.
20. Alvarez, L. J., Leon, L. E., Sanz, J. F., Capitan, M. J. and Odriozola, J. A., Micropore formation mechanisms in γ-Al_2O_3. *Surface Science*, 1995, **322**, 185–192.
21. Selvaraj, U., Komarneni, S. and Roy, R., Synthesis of glass-like cordierite from metal alkoxides and characterization by ^{27}Al and ^{29}Si MASNMR. *J. Am. Ceram. Soc.*, 1990, **73**, 3663–3669.
22. Brese, N. E. and O'Keeffe, M., Bond-valence parameters for solids. *Acta Cryst.*, 1991, **B47**, 192–197.

23. Oudet, F., Courtine, P. and Vejux, A., Thermal stabilization of transition alumina by structural coherence with $LnAlO_3$ (Ln = La, Pr, Nd). *J. Catalysis*, 1988, **114**, 112–120.
24. Lin, Y.-S., Chang, C.-H. and Gopalan, R., Improvement of thermal stability of porous nanostructured ceramic membranes. *Ind. Eng. Chem. Res.*, 1994, **33**, 860–870.
25. Ozawa, M., Kimura, M. and Isogai, A., Thermal stability and characterization of γ-Al_2O_3 modified with lanthanum or cerium. *J. Mater. Sci. Let.*, 1990, **9**, 709–711.
26. Thompson, P., Cox, D. E. and Hastings, J. B., Rietveld refinement of Debeye-Scherreer synchrotron X-ray data from Al_2O_3. *J. Appl. Crystallography*, 1987, **20**, 79–83.